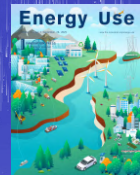


Energy Use

Energy Use 1 (2025):100009

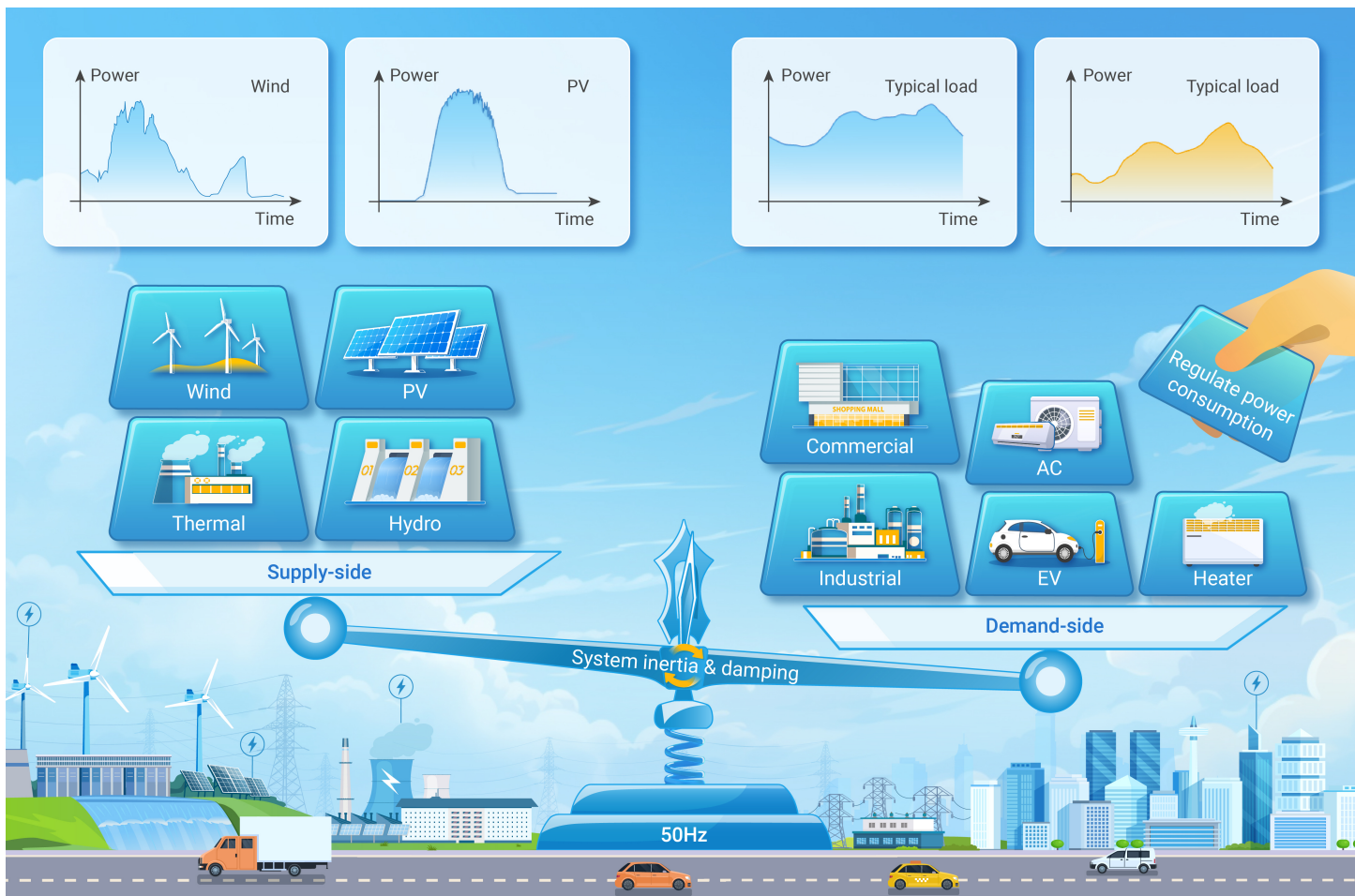
Contents lists available at INNOVATION PRESS



Equivalence of Inverter Air Conditioners as Virtual Synchronous Generators for Enhancing Power System Inertia and Frequency Stability

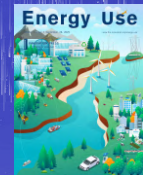
Hongxun Hui^{1,*} and Yonghua Song¹*Correspondence: hongxunhui@um.edu.moReceived: September 2, 2025; Accepted: September 22, 2025; Published Online: September 25, 2025; <https://doi.org/10.59717/ijp.energy-use.2025.100009>© 2025 The Author(s). This is an open access article under the CC BY license (<https://creativecommons.org/licenses/by/4.0/>).

GRAPHICAL ABSTRACT



PUBLIC SUMMARY

- Proposes controlling inverter air conditioners (IACs) as virtual synchronous generators (VSGs) to enhance power system frequency stability.
- A control scheme that ensures IACs provide inertia and damping while maintaining comfortable temperature limits.
- A dynamic evaluation method and flexible parameter configuration for IAC-VSG controllers, validated by numerical studies.



Equivalence of Inverter Air Conditioners as Virtual Synchronous Generators for Enhancing Power System Inertia and Frequency Stability

Hongxun Hui^{1,*} and Yonghua Song¹¹Science and Technology Research Institute, University of Macau, Macau 999078, China*Correspondence: hongxunhui@um.edu.moReceived: September 2, 2025; Accepted: September 22, 2025; Published Online: September 25, 2025; <https://doi.org/10.59717/ijpj.energy-use.2025.100009>© 2025 The Author(s). This is an open access article under the CC BY-NC-ND license (<https://creativecommons.org/licenses/by/4.0/>).Citation: and Song Y. (2025). Equivalence of Inverter Air Conditioners as Virtual Synchronous Generators for Enhancing Power System Inertia and Frequency Stability. *Energy Use* 1:100009.

The increasing penetration of renewable energies is decreasing modern power systems' inertia and damping rapidly, which threatens the safe and stable operation of the power system. Considering inverter air conditioners (IACs) account for more than 30% of the total power consumption and have huge regulation potential, this paper proposes to control IACs as virtual synchronous generators (VSGs), named IAC-VSG resources, to provide additional inertia and damping for frequency stability enhancement. A simple but widely adaptable control scheme for general IACs supporting frequency response is developed by modifying the active power reference. The modified IACs can not only provide inertia and damping as VSGs do, but also remain user-friendly by maintaining comfortable temperature limits in the control model. To quantify the dynamic performance of the power system after integrating IAC-VSGs, a dynamic evaluation method is proposed via the closed-loop transfer function in the complex frequency domain, including the resonant frequency, peak value, and 2-norm. On this basis, a parameter configuration method for IAC-VSG controllers is designed to flexibly adjust the equivalent inertia and damping ratios according to different power system requirements. Finally, numerical studies verify the effectiveness of the proposed methods.

INTRODUCTION

Renewable energies (RENs), such as photovoltaics and wind power generation, are increasing rapidly in modern power systems to reduce carbon emissions.¹ Meanwhile, the phasing-out of traditional synchronous generators (SGs) is accelerating the change of the power system from SGs-dominated to RENs-dominated.² Traditional SGs (e.g., thermal power generators) have large rotating mass and are the main contributors of the system inertia and damping nowadays, which determine the system's disturbance rejection ability.³ By contrast, RENs are generally interfaced with the power system via power electronics, which have very small or no rotating mass.⁴ Therefore, the system equivalent inertia and damping are decreasing along with the replacement of SGs by RENs, which threatens the safe and stable operation of the power system.⁵

The progressed Internet of Things makes it possible to control flexible loads on the demand side to provide regulation services for the power system.⁶ Among different kinds of flexible loads, air conditioners (ACs) are important and have huge regulation potentials,⁷ because they account for a large proportion of the total loads (e.g., more than 60% in many cities around the world).⁸ Furthermore, the indoor temperature can be guaranteed in comfortable ranges during the regulation process by utilizing buildings' thermal storage characteristics.⁹ Therefore, ACs are suitable to provide regula-

tion services for the power system.¹⁰ Lu¹¹ proposes a temperature-priority-list method to control air conditioners (ACs), in which the ACs' regulation potential is evaluated and proven to be compatible with the power system's dispatch requirements. Chen et al.¹² developed a reinforcement learning method to control ACs for providing regulation services, ensuring that the required indoor temperature is always maintained. Compared with regular fixed-speed ACs that only operate in on/off states, inverter air conditioners (IACs) can adjust their operating power continuously from zero to the rated value.¹³ Hence, IACs offer more flexibility to provide regulation services for the power system.¹⁴ Furthermore, the number of installed IACs has surpassed the number of regular fixed-speed ACs in many countries around the world,¹⁵ highlighting their larger regulation potential and increasing attention to them. Song et al.¹⁶ propose a multi-time-scale coordinated control and scheduling strategy for IACs to compensate for tie-line power flow deviations caused by wind generation. This demonstrates that the power consumption of IACs can be smoothly regulated. Zhang et al.¹⁷ develop a plug-and-play learning framework to automatically identify the building's thermal model and control the IACs in commercial buildings for providing cost-effective regulation services. Kim et al.¹⁸ propose a direct load control method to regulate IACs every four seconds, verifying that IACs can be flexibly controlled in multiple time scales. In addition, some incentive methods¹⁹ and optimal bidding methods²⁰ have been studied to reduce IACs' energy costs and increase regulation benefits. IACs are modeled and controlled to provide frequency regulation services for the power system, where communication latency is also considered.²¹ Although these studies demonstrate that IACs are good regulation resources, to the best of our knowledge, no research has been done to control IACs to emulate traditional synchronous generators (SGs) properties to improve system equivalent inertia and damping. This is referred to as IAC-based virtual synchronous generators (IAC-VSGs).²² This research gap is the focus of this paper: developing the model and control methods of IAC-VSGs to enhance RENs-dominated power system stability.²³ However, compared with the inertia and damping provided by traditional SGs,²⁴ the effects of IAC-VSGs on the power system's dynamic performance are complex to evaluate. This also increases the modeling and control difficulties of IAC-VSGs. For example, in traditional SGs-dominated power systems, the system's dynamic performance is generally evaluated by the system inertia H ,²⁵ which can be calculated through the weighted average of all the online SGs as follows:

$$H \cdot S = \sum_{j \in J} H_j^G \cdot S_j^G, \quad (1)$$

The total capacity of the SGs within the power system is denoted as S .

Symbols H_j^g and S_j^g represent the inertia ratio and the rated capacity of the j -th SG, respectively, which can be obtained by the system operator.²⁶ Therefore, the system equivalent inertia H can be accurately evaluated by monitoring the online number of SGs.²⁷ By contrast, the equivalent inertia of one IAC-VSG is not a fixed value. Instead, it is time-varying and nonlinear with respect to the IACs' operation states,²⁸ including dynamic indoor temperatures, ambient temperatures, user-defined comfortable temperature settings, and the thermal characteristics of buildings.²⁹ Furthermore, the online number of IAC-VSGs is also uncertain, which implies that the system equivalent inertia considering IAC-VSGs cannot be evaluated using the method in Equation (1).

Faced with the above issues, this paper aims to explore the substantial regulation potential of inverter air conditioners (IACs) in improving the dynamic performance of renewable energy-dominated power systems. First, the thermal and electrical models of IACs are transformed from the time domain into the complex frequency domain. Then, the equivalent model of IAC-VSGs and the closed-loop transfer function model of the novel power system incorporating IAC-VSGs are derived. On this basis, an evaluation method in the complex frequency domain is proposed to quantify the system's dynamic performance, including the resonant frequency, the resonant peak value, and the H_2 -norm.³⁰ The main contributions of this study are as follows:

1. We derive a modification method for IACs based on the existing IAC control framework. By adding a PD controller to adjust the active power reference within comfortable temperature range, the modified IAC model is derived to be equivalent as VSGs to improve system inertia and damping ratios for frequency stability enhancement.

2. We develop the closed-loop transfer function of the novel system model with IAC-VSGs in the complex frequency domain. On this basis, we also propose an evaluation method about the dynamic performance to quantify the power system rejection ability on disturbances considering IAC-VSGs, including the resonant frequency, the peak value, and 2-norm.

3. We design a configuration method for the control parameters of IAC-VSGs to achieve a flexible adjustment of the equivalent inertia and damping subject to power system requests. The method can effectively restore the system rejection ability on stochastic disturbances.

MATERIALS AND METHODS

Equivalent modelling and control of IAC as VSG

Modelling of IAC. The thermal model of a room installed with an IAC can be developed as follows:¹⁵

$$C_i \frac{d\theta_i(t)}{dt} = \frac{\theta_o(t) - \theta_i(t)}{R_i} - Q_i(t), \quad \forall i \in I, \quad (2)$$

where I is the set of rooms and corresponding IACs; C_i and R_i are the thermal capacity and resistance of the room, respectively; $\theta_i(t)$ and $\theta_o(t)$ are the real-time indoor temperature and ambient temperature, respectively; $Q_i(t)$ is the cooling capacity, which can be calculated by IAC's coefficient of performance and its operating power $P_i(t)$:

$$Q_i(t) = \eta P_i(t), \quad \forall i \in I, \quad (3)$$

For illustrating the thermal dynamic process more clearly, we transfer the Equations (2)-(3) from the time domain to complex frequency domain via *Laplace Transform*, as follows:

$$\theta_i(s) = \frac{1}{1+C_i R_i s} [\theta_o(s) - R_i \eta \cdot P_i(s)], \quad \forall i \in I, \quad (4)$$

where s is the Laplace operator. Equation (4) illustrates that the indoor temperature $\theta_i(s)$ deviates with the ambient temperature $\theta_o(s)$ and the operating power $P_i(s)$. The indoor temperature will be higher with the increase of the ambient temperature or the decrease of the operating power.

Control of IAC. From the control perspective, the IAC should have the function of maintaining the indoor temperature θ_i in a comfortable range. In other words, the indoor temperature is required to be regulated by the IAC as equal to the set temperature θ_i^{set} . When the indoor temperature θ_i appears deviations or the set value θ_i^{set} is adjusted by users, the IAC's operating power will be adjusted from the initial stable state according to the difference between θ_i and θ_i^{set} , as follows:

$$\Delta P_i(s) = P_i^N \phi(s) [\Delta \theta_i(s) - \Delta \theta_i^{\text{set}}(s)], \quad \forall i \in I, \quad (5)$$

where P_i^N and $\phi(s)$ are the rated power and the built-in controller of the IAC, respectively.

In this paper, we want to control IACs as VSGs to enhance the power system stability. Therefore, apart from the built-in controller $\phi(s)$, another controller should be designed to regulate the IAC's operating power according to the power system's states. Inspired from the control method of wind turbines and solar photovoltaics as VSG, the method by modifying the active power reference (MAPR) is adopted here to control IAC-VSG,³¹ which is expressed as:

$$P_i^{\text{ref}}(t) = P_i^0 + K_{\text{VSG}} \frac{f(t) - f_r}{f_r} P_i^N + T_{\text{VSG}} \frac{df(t)}{dt} P_i^N, \quad \forall i \in I, \quad (6)$$

where $P_i^{\text{ref}}(t)$ is the reference value of the IAC's active power for emulating VSG; P_i^0 is the initial active power of the IAC, i.e., the operating power at the beginning of control; $f(t)$ and f_r are the system's frequency in real time and its rated value, respectively; K_{VSG} and T_{VSG} are the two control coefficients to regulate IAC's active power for imitating VSG.

Based on the Equation (6), we can obtain the feedback control of IAC's operating power based on the power system's frequency signals. The regulation quantity of the IAC's power can be also deduced in complex frequency domain:

$$\Delta P_i(s) = L [P_i^{\text{ref}}(t) - P_i^0] = P_i^N (K_{\text{VSG}} + T_{\text{VSG}} s) \Delta f(s), \quad \forall i \in I, \quad (7)$$

where L indicates the *Laplace Transform*. $\Delta f(s)$ is the per unit value of the power system's frequency deviation:

$$\Delta f(s) = L [(f(t) - f_r)/f_r]. \quad (8)$$

Combining Equations (5) and (7) can obtain the regulation quantity of the IAC's active power considering the VSG function:

$$\Delta P_i(s) = P_i^N \phi(s) [\Delta \theta_i(s) - \Delta \theta_i^{\text{set}}(s)] + P_i^N (K_{\text{VSG}} + T_{\text{VSG}} s) \Delta f(s), \quad \forall i \in I. \quad (9)$$

The Equation (9) means that the IAC's power can be regulated by two controllers: the built-in controller $\phi(s)$ for adjusting the indoor temperature and the external controller ($K_{\text{VSG}} + T_{\text{VSG}} s$) for providing VSG support to the power system.

Substituting Equation (4) into Equation (9) yields:

$$\begin{aligned} \Delta P_i(s) &= P_i^N \phi(s) \Delta \theta_o(s) - (1+C_i R_i s) \phi(s) \Delta \theta_i^{\text{set}}(s) \\ &\quad + P_i^N \frac{(1+C_i R_i s)(K_{\text{VSG}} + T_{\text{VSG}} s) \Delta f(s)}{1+C_i R_i s + \eta R_i P_i^N \phi(s)}, \quad \forall i \in I. \end{aligned} \quad (10)$$

The Equation (10) indicates that the IAC's regulation quantity depends on three changes: the outdoor temperature $\Delta \theta_o(s)$, the user's set temperature $\Delta \theta_i^{\text{set}}(s)$, and the system's frequency deviation $\Delta f(s)$. When the ambient temperature increases (i.e., $\Delta \theta_o(s) > 0$) or the set temperature is turned down by users (i.e., $\Delta \theta_i^{\text{set}}(s) < 0$), the IAC will increase its power consumption. Furthermore, the IAC in this paper is also regulated with the system frequency deviations $\Delta f(s)$. When the system frequency is less than the rated value (i.e., $\Delta f(s) < 0$), the IAC will decrease its power consumption. It is equivalent to increasing the power output from generators to provide regulation services. Considering the short time period of IACs for providing regulation power as VSG (generally within 30s-5min),¹⁵ the outdoor temperature can be regarded as a constant (i.e., $\Delta \theta_o(s) = 0$). Besides, most of users do not frequently adjust the set temperature, which is also assumed to be fixed during the regulation period (i.e., $\Delta \theta_i^{\text{set}}(s) = 0$). Then we can neglect the two variables $\Delta \theta_o(s)$ and $\Delta \theta_i^{\text{set}}(s)$ in Equation (10) to get the simplified form of IAC-VSG's regulation power:

$$\begin{aligned} \Delta P_i^{\text{VSG}}(s) &\approx P_i^N \frac{(1+C_i R_i s)(K_{\text{VSG}} + T_{\text{VSG}} s) \Delta f(s)}{1+C_i R_i s + \eta R_i P_i^N \phi(s)} \\ &= \psi_i(s) (K_{\text{VSG}} + T_{\text{VSG}} s) \Delta f(s), \quad \forall i \in I, \end{aligned} \quad (11)$$

where $\psi_i(s)$ represents the IAC-VSG model:

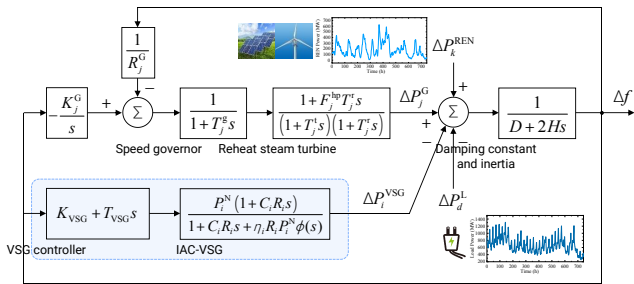


Figure 1. The power system model with traditional generating units, renewable energies, and IAC-VSGs.

$$\psi_i(s) = \frac{P_i^N(1+C_iR_iS)}{1+C_iR_iS+\eta_iR_iP_i^N\phi(s)}, \forall i \in I. \quad (12)$$

Comfort limits. The proposed IAC control framework is expected to provide a frequency support for power systems while maintaining user comfort. To ensure the user comfort, indoor temperature needs to be maintained around the set temperature, expressed as $\theta_i^{\text{set}} \pm \Delta\theta_c$, where $\Delta\theta_c$ is a pre-defined value to describe the range of users' comfortable temperature. As for an IAC operating in the stable state (i.e., the indoor temperature is maintained to be equal to the set value), the upper and lower bound of the IAC power considering user comfort can be expressed as follows:

$$P_i^{\text{upper/lower}}(t) = \frac{\theta_i(t) - \theta_i^{\text{set}}(t) \pm \Delta\theta_c}{\eta_i R_i}, \quad \forall i \in I. \quad (13)$$

Modelling of the power system integrated with IAC-VSGs. This subsection integrates the proposed IAC-VSG into the traditional power system model, as shown in Figure 1. The system frequency deviation Δf is influenced by fluctuating renewable energies P_k^{REN} and loads ΔP_d^L , and then regulated by SGs ΔP_j^G and VSG ΔP_i^{VSG} . Hence, the system frequency deviation can be expressed as:

$$\Delta f(s) = \frac{1}{D+2Hs} \left[\sum_{j \in J} \Delta P_j^G(s) + \sum_{k \in K^C} \Delta P_k^{\text{REN}}(s) - \sum_{i \in I} \Delta P_i^{\text{VSG}}(s) - \sum_{d \in D} \Delta P_d^L(s) \right]. \quad (14)$$

where D and H are the damping and inertia ratios of the system, respectively.

Substituting Equation (11) into Equation (14) yields:

$$\Delta f(s) = \frac{1}{D(s)+2H(s)s} \left[\sum_{j \in J} \Delta P_j^G(s) + \sum_{k \in K} \Delta P_k^{\text{REN}}(s) - \sum_{d \in D} \Delta P_d^L(s) \right], \quad (15)$$

where $D(s)$ and $H(s)$ represent the equivalent damping and inertia of the power system with IAC-VSGs, respectively.

These two equivalent values can be expressed as:

$$\begin{cases} D(s) = D + K_{\text{VSG}} \sum_{i \in I} \psi_i(s), \\ H(s) = H + \frac{T_{\text{VSG}}}{2} \sum_{i \in I} \psi_i(s). \end{cases} \quad (16)$$

Remark 1. Equation (16) proves that the system equivalent damping and inertia are the summation of the system original dynamic performance (i.e., damping D and inertia H) and the additional supports from IAC-VSGs. In other words, the proposed IAC-VSG model and MAPR control method can effectively enhance the system damping ratio D and inertia H . It is important for modern power systems with lower inertia due to high penetration of power electronics-interfaced RENs.

Dynamic performance quantification and parameter configuration methods for IAC-VSGs

It is proved that the power system's stability can be enhanced by IAC-VSG in Section II, while how to configure appropriate control parameters for IAC-VSGs (i.e., K_{VSG} and T_{VSG}) is another problem. To address this issue, the power system's dynamic performance with changes of damping $D(s)$ and inertia ratios $H(s)$ should be quantified first. In this section, we propose a quantitative evaluation method to characterize IAC-VSGs' effects on the system stability based on the power system's closed-loop transfer function.³⁰ The configuration method for IAC-VSGs' control parameters is also designed in

this section to make up for the power system's dynamic performance.

Quantification of the system dynamic performance. Here we employ the power system's closed-loop transfer function to quantify the influence of damping and inertia ratios on the system's dynamic performance. As shown in Figure 1, the system has two disturbances (i.e., fluctuating RENs and loads), which can be expressed as:

$$\Delta P^{\text{dist}}(s) = \sum_{k \in K^C} \Delta P_k^{\text{REN}}(s) - \sum_{d \in D} \Delta P_d^L(s). \quad (17)$$

Note that this paper assumes RENs operate in the maximum power point tracking mode and have no regulation capacities. In this manner, we can focus on analyzing the regulation effect from the proposed IAC-VSGs.

The regulation power from SGs in Figure 1 can be expressed as:

$$\Delta P_j^G(s) = -G_j(s)\Delta f(s), \forall i \in I, \quad (18)$$

where $G_j(s)$ is the transfer function of the j -th SG:¹⁵

$$G_j(s) = \left(\frac{1}{R_j^G} + \frac{K_j^G}{s} \right) \frac{1}{1+T_j^G s} \cdot \frac{1+T_j^{\text{hp}} T_j^s}{(1+T_j^s)(1+T_j^{\text{r}} s)}, \forall j \in J. \quad (19)$$

where R_j^G and K_j^G are the control coefficients for providing primary and secondary regulation services, respectively; T_j^G s, T_j^s and T_j^{r} s are time constants of the speed governor, turbine and reheat process, respectively; T_j^{hp} is the high pressure turbine section.

Based on Equations (15)-(19), we can obtain the closed-loop transfer function of the system frequency deviations relating to the disturbances, as follows:

$$TF(s) = \frac{\Delta f(s)}{\Delta P^{\text{dist}}(s)} = \frac{1}{D(s)+2H(s)s+\sum_{j \in J} G_j(s)}. \quad (20)$$

Then we employ Bode plots of the closed-loop transfer function in Equation (20) to characterize the effects of different damping and inertia ratios on the system's dynamic performance. Figure 2A shows Bode plots of power systems with the same damping ratio (i.e., $D(s) = 1$) while different inertia ratios (i.e., $H(s) = 10, 1$). By contrast, Figure 2B shows Bode plots of power systems with the same inertia ratio (i.e., $H(s) = 10$) while different damping ratios (i.e., $D(s) = 1, 0.1$). Other parameters are explained in detail in APPENDIX A. Note that the regulation effect from IAC-VSGs is not considered in these two figures (i.e., $D(s) = D$, and $H(s) = H$).

The results in Figure 2A illustrate that the resonant frequency f^{res} and corresponding resonant peak value p^{res} increase with the decrease of inertia ratio H . For example, the resonant frequency and peak value in the first scenario ($H = 10$) are 0.43Hz and -17.39dB, while they are enlarged to 2.67Hz and -7.95dB in the last scenario ($H = 1$), respectively. Based on control theories,³⁰ the resonant frequency f^{res} and corresponding peak value p^{res} can characterize the system's disturbance rejection ability on resonant frequency, which is weakened by the decrease of inertia ratio H . By contrast, Figure 2B indicates that only the resonant peak value p^{res} gets increased with the decrease of damping ratio D , while the resonant frequency f^{res} remains unchanged. Therefore, we can get the following monotonic increasing relation functions:

$$\begin{cases} f^{\text{res}} = f(H(s)), \\ p^{\text{res}} = g(H(s), D(s)). \end{cases} \quad (21)$$

Remark 2. The resonant frequency of the system's closed-loop transfer function (i.e., f^{res}) depends on the inertia ratio $H(s)$ while it is independent of the damping ratio $D(s)$. The resonant peak value (i.e.,

p^{res}) is related to both the inertia ratio $H(s)$ and the damping ratio $D(s)$. Therefore, if we want to restore the power system's disturbance rejection ability on resonant frequency to the required value, the inertia ratio $H(s)$ can be regulated first to restore the system resonant frequency f^{res} . Then the damping ratio $D(s)$ can be regulated to restore the system resonant peak value p^{res} .

Apart from the above two indexes f^{res} and p^{res} to quantify the system's disturbance rejection ability on resonant frequency, we employ the H_2 norm to characterize the system's disturbance rejection ability on the full-band. The H_2 norm is defined as the root-mean-square of the power system's

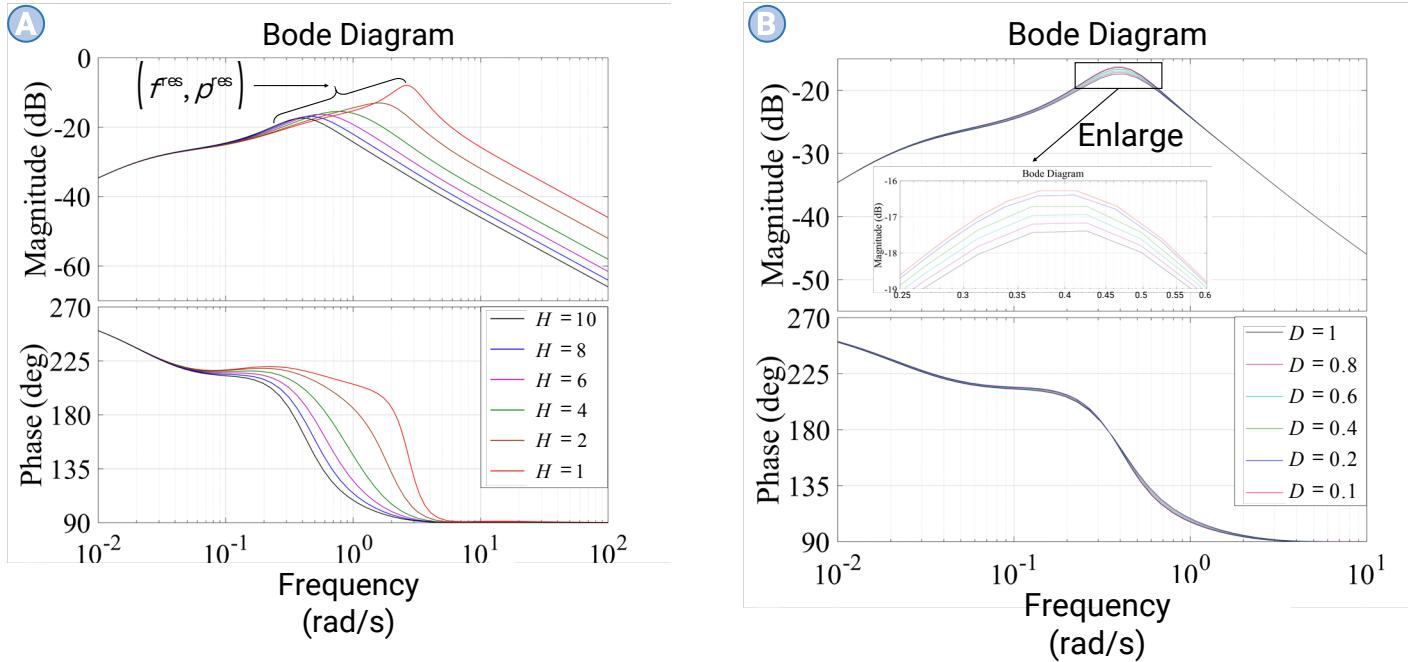


Figure 2. Bode plots of the power system. (A) Scenarios of different inertia ratios. (B) Scenarios of different damping ratios.

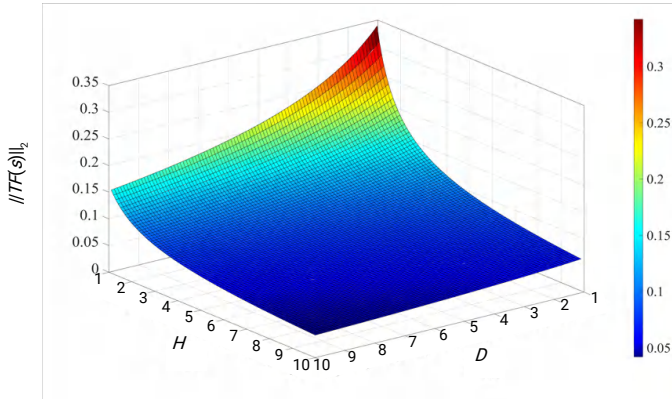


Figure 3. The H_2 norm of the system's closed-loop transfer function with different damping and inertia ratios.

impulse response, and can be calculated as:

$$\|TF(s)\|_2 = \sqrt{\frac{1}{2\pi} \int_{-\infty}^{\infty} \text{tr}[TF(j\omega)^H TF(j\omega)] d\omega}, \quad (22)$$

where $\text{tr}[A]$ and A^H represent the trace and conjugate transpose of matrix A , respectively. Figure 3 shows the H_2 norm values of the system's closed-loop transfer function with different damping and inertia ratios. It can be seen that the H_2 norm will be smaller with the increase of damping and inertia ratios. Therefore, the power system with smaller H_2 norm has stronger disturbance rejection ability on the full-band. Besides, Figure 3 illustrates that damping and inertia ratios are interchangeable to some degree for decreasing H_2 norm and enhancing the power system's stability. However, compared with damping ratio, the H_2 norm drops faster with the change of inertia in Figure 3. It means that the inertia can play a greater value to increase the system's disturbance rejection ability on the full-band. Based on the above analysis, we can get the following monotonic decreasing relation function:

$$H_2 = h(H(s), D(s)). \quad (23)$$

Remark 3. The H_2 norm depends on the system's inertia ratio $H(s)$ and damping ratio $D(s)$, which is monotonically decreasing with both $H(s)$ and $D(s)$. Therefore, if we want to restore the power system's disturbance rejection ability on the full-band, the inertia and damping ratios can be both regulated to achieve the stability requirement.

To sum up, this subsection proposes the resonant frequency f^{res} , resonant peak value p^{res} , and H_2 norm to quantify the system's dynamic performance, i.e., the system's disturbance rejection ability on resonant and full-band frequencies. The control objective of IAC-VSGs is to assist the RENs-dominated power system to restore these quantitative indexes by configuring the control parameters K_{VSG} and T_{VSG} .

Configuration of IAC-VSG Control Parameters. Two typical power systems with insufficient inertia and damping ratios are analyzed in Figure 4A and Figure 4B, respectively. Assuming the original power system's inertia and damping ratios are 10 and 1, respectively. The inertia ratio decreases to 6 in Figure 4A, and the damping ratio decreases to 0.6 in Figure 4B. Other parameters of the power system are explained in detail in APPENDIX A. The parameters of IAC-VSGs are shown in APPENDIX B.

Figure 4A illustrates that the Bode curve moves from the dotted line to the dash-dotted line when the inertia ratio decreases from 10 to 1. However, it can be pulled back by increasing the control parameter T_{VSG} of IAC-VSGs, i.e., the red line coincides with the original black dotted line. The resonant frequency f^{res} and resonant peak value p^{res} are also decreased back to the original values. Besides, f^{res} and p^{res} keep decreasing with the increase of T_{VSG} , and can even exceed the original values (e.g., the green curve). It means that the power system's disturbance rejection ability on resonant frequency can not only be restored, but also be adjusted flexibly to meet the system's different requirements by configuring the control parameter T_{VSG} .

Figure 4B illustrate that the increased resonant peak value p^{res} caused by smaller damping ratio can be pulled back by IAC-VSGs, i.e., the red line coincides with the original black dotted line. The H_2 norm is also restored from 0.0649 in the second scenario ($D = 0.6$, without IAC-VSGs) to 0.0631 in the fifth scenario ($D = 0.6$, with IAC-VSGs, $K_{VSG} = 50$). It is equal to the original H_2 norm in the first scenario ($D = 1$, without VSG). Besides, we can see that the resonant frequency remains unchanged in different values of the parameter. Therefore, Figure 4A and Figure 4B verify the relation functions in Equations (21) and (23). It proves that IAC-VSGs can restore the system's dynamic performance on rejecting different kinds of disturbances. As for a realistic power system with changeable inertia and damping ratios in different operation periods, the dynamic performance should be maintained by configuring the two control parameters (i.e., K_{VSG} and T_{VSG}) at the same time. Based on the Equation (21), we know that the system's resonant frequency only depends on the inertia. Therefore, can be designed first to restore the deviated resonant frequency f^{res} . From Equations (16) and (21), T_{VSG} can be expressed as the inverse function of f^{res} :

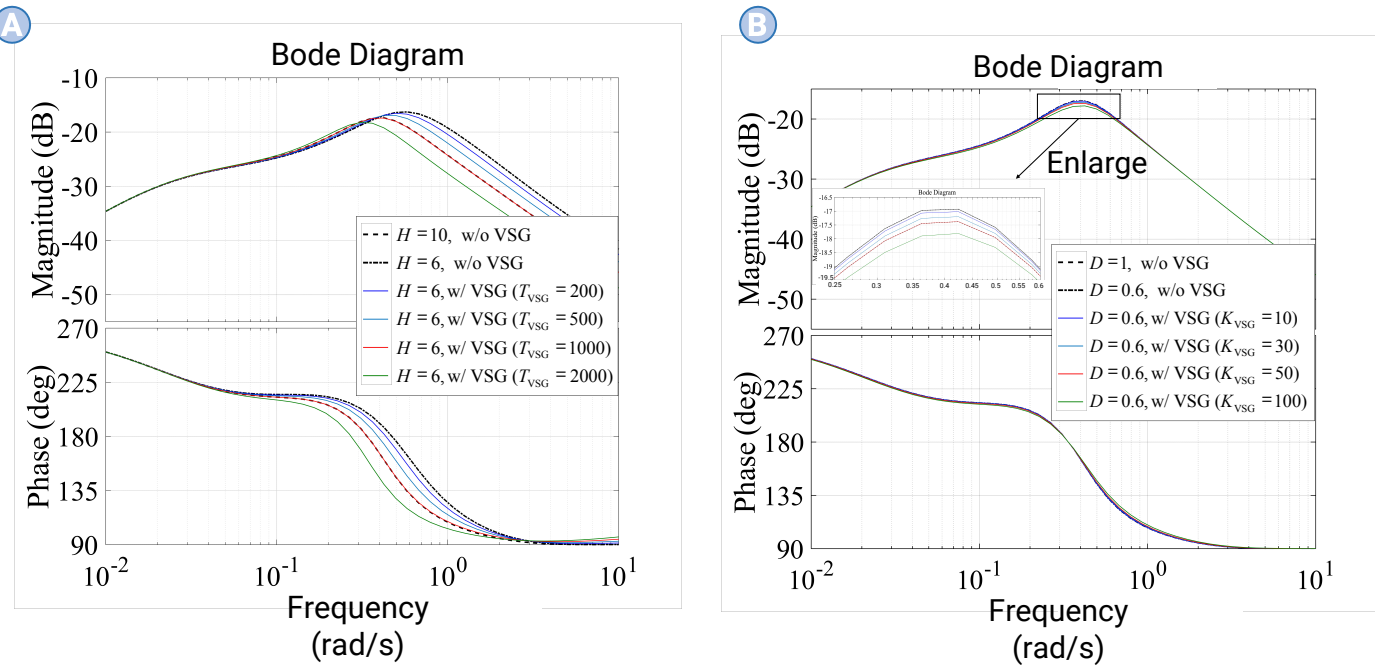


Figure 4. Bode plots of the power system with IAC-VSGs. (A) Scenarios of different T_{vsg} . (B) Scenarios of different K_{vsg} .
 $T_{vsg} = f^{-1}(f^{res})$. (24)

Based on the designed value of T_{vsg} , the other control parameter K_{vsg} can then be configured to restore the H_2 norm for recovering the system's disturbance rejection ability on the full-band. From Equations (16) and (23), K_{vsg} can be expressed as the inverse function of H_2 norm and T_{vsg} :

$$K_{vsg} = h^{-1}(H_2, T_{vsg}). \quad (25)$$

In this manner, the two control parameters for IAC-VSGs can be set to restore the two disturbance rejection abilities on resonant and full-band frequency. The configuration process for IAC-VSG is shown as:

01 Initialization: Based on the power system's parameters, calculate the initial resonant frequency f^{res} , resonant peak value p^{res} , and H_2 norm to quantify the system's dynamic performance. These indexes are regarded as the system's required disturbance rejection ability. Assuming the initial number of SGs is J_0 .

02 For $t = 0:1:T$ do

03 Monitor the online number of SGs J_t , because some SGs may be shut down in some dispatch periods with the fluctuating power output of RERs.

04 If $J_t < J_0$ then

05 Detect the online adjustable IACs, and calculate the thermalelectrical model $\psi_i(s)$ based on Equation (12).

06 Configure the control parameter T_{vsg} for IAC-VSGs to restore the system's disturbance rejection ability on resonant frequency based on Equations (11)-(21), (24).

07 Configure the control parameter K_{vsg} for IAC-VSG to restore the system's disturbance rejection ability on the full band based on Equations (11)-(20), (22)-(25).

08 Else

09 Configure the control parameters as, $T_{vsg} = K_{vsg} = 0$ and do not need IACs to provide regulation services.

10 End if

11 Terminal controllers of IAC-VSGs receive the control parameters T_{vsg} and K_{vsg} from the dispatcher.

12 Terminal controllers monitor the power system's frequency deviation Δf in real time.

13 If $\Delta f > \Delta f^{thr}$ then

14 Terminal controllers regulate IAC-VSGs to provide regulation services for the power system based on the Equation (11).

15 End if

16 End for

RESULTS

Numerical studies

Test System. The total installed capacity of the power system is 8,000MW with 10 reheat steam SGs, whose parameters are shown in detail in APPENDIX A. The rated frequency of the power system is 50Hz. The parameters of the adjustable IACs are based on the Chinese National Standards and some realistic test data, as shown in APPENDIX B. The total operating power of IACs accounts for around 7% of the power system's capacity. The threshold of system frequency deviation f^{thr} for regulating

IAC is set as 0.05Hz. Besides, to compare the traditional SGs-dominated power system and the high-penetration RENs-dominated power system, the installed RENs are assumed to account for 40% of the total installed capacity.³² Based on the above parameters, assuming 5% load power is added abruptly to the power system. Then we can analyze the system's dynamic performance and frequency deviations. The models and methods are formulated in MATLAB R2019b on a computer with Intel(R) Core (TM) i7-9700 CPU, clocking at 3.00GHz and 16.0GB RAM.

Result Analysis on the System Dynamic Performance. Figure 5 shows the system frequency deviations to analyze different power systems' dynamic performance under the same load disturbance in time domain. Figure 5A & B illustrate that the maximum frequency deviation (i.e., frequency nadir f^{nadir}) drops to a lower value with the decrease of inertia H and damping D . For example, as shown in Figure 5A and Table S1, f^{nadir} decreases from -0.234Hz to -0.545Hz when H decreases from 10 to 1. As shown in Figure 5B and Table S1, f^{nadir} decreases from -0.134Hz to -0.252Hz when D decreases from 10 to 0.1. It indicates that the system's dynamic performance is weakened due to the decrease of inertia H and damping D . However, H and D have different effects on the fall time Δt^{nadir} (i.e., the period from the beginning of frequency deviations to the frequency nadir). In Figure 5A, the fall time Δt^{nadir} becomes shorter with the decrease of H , which is 3.64s in $H=10$ scenario and shortened to 0.74s in $H=1$ scenario. Therefore, the rate of change of frequency (RoCoF) becomes steeper with the decrease of H , as shown in Table S1. It is harmful for the power system to deal with contingencies. More seriously, the system frequency even appears oscillations in $H=1$ scenario, which indicates the power system becomes more volatile. By contrast, in Figure 5B, the Δt^{nadir} becomes longer with the decrease of D , which is 2.65s in $D=10$ scenario and extended to 3.79s in $D=0.1$ scenario. This means that a smaller D can only reduce the frequency nadir Δf^{nadir} , while almost has no impact on the RoCoF, as shown in Table S1. Hence, compared with the decrease of inertia, the diminished damping ratio reserves longer time for the power system to deal with disturbances.

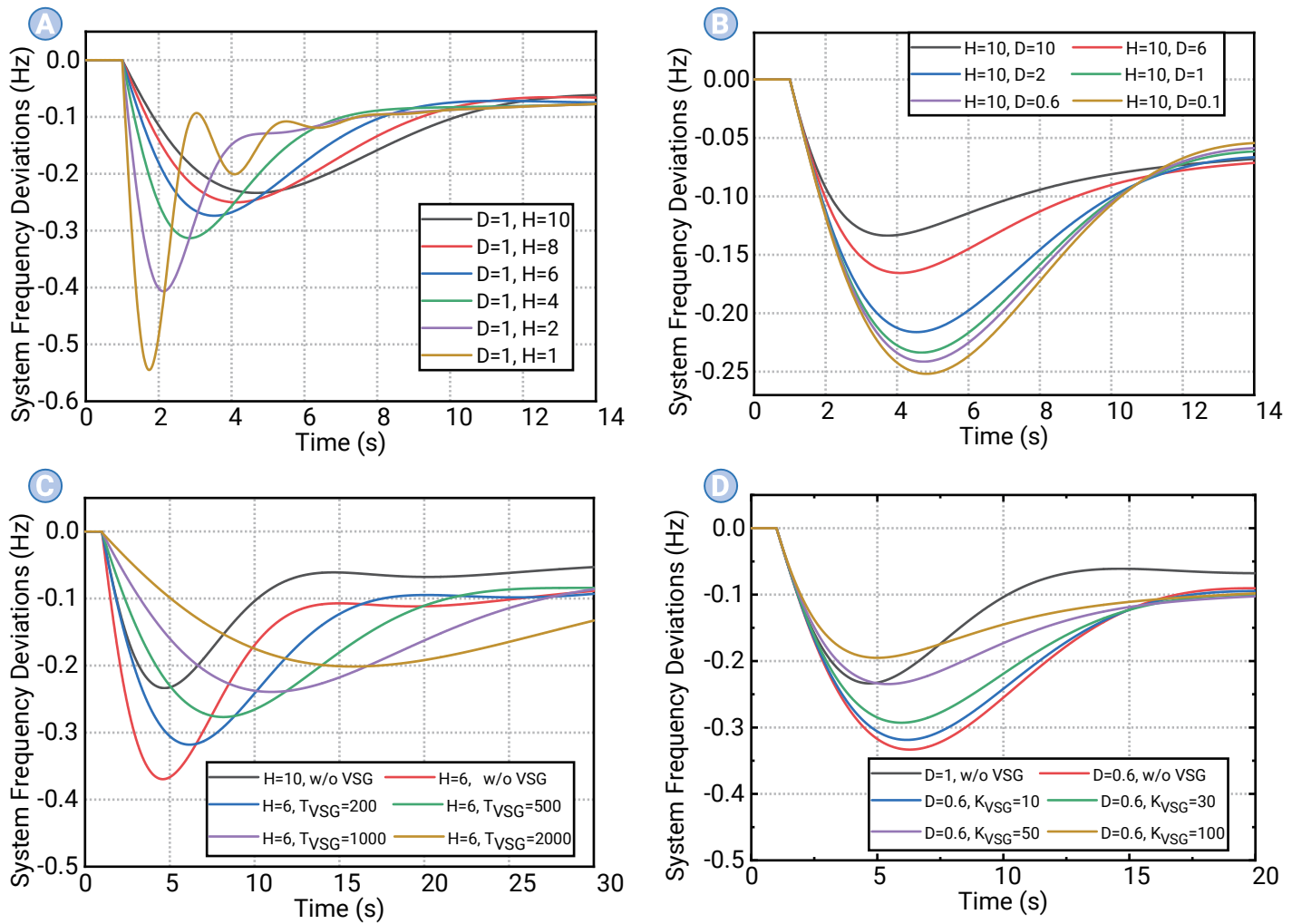


Figure 5. System frequency deviations under load disturbances (A) Power systems with the same damping ratio $D = 1$ while different inertia $H = 10 \sim 1$. (B) Power systems with the same inertia $H = 1$ while different damping ratios $D = 10 \sim 0.1$. (C) Configuration of IAC-VSGs in power systems with the same damping ratio $D = 1$ while decrescent inertia $H = 6$. (d) Configuration of IAC-VSGs in power systems with the same inertia $H = 10$ while decrecent damping ratio $D = 0.6$.

To compensate for the system's dynamic performance in Figure 5A & B, IAC-VSGs are controlled in Figure 5C & D to increase the system equivalent inertia and damping ratios. Figure 5C illustrates that the Δf^{nadir} can be restored to the original value -0.234Hz by configuring the IAC-VSG's control parameter T_{VSG} . Besides, the RoCoF can also be slowed down by increasing the equivalent inertia, which makes up for the fast frequency drop caused by diminished H . Figure 5D illustrates the Δf^{nadir} can be restored by configuring the IAC-VSG's control parameter K_{VSG} , where the RoCoF keeps almost unchanged.

To sum up, the decrease of inertia and damping ratios can weaken the system's dynamic performance, while it can be compensated by IAC-VSGs to increase the Δf^{nadir} and alleviate the RoCoF.

Result analysis on the power system regulation with smaller inertia and damping ratios. As for a realistic power system, the inertia and damping ratios probably change at the same time. In this condition, the two control parameters T_{VSG} and K_{VSG} of the IAC-VSGs can be configured based on the proposed method in Table I. The process is shown in Figure 6, where H and D decrease from 10 and 1 to 6 and 0.6, respectively. It causes the Bode plot moves from the original black curve to the cyan curve. Then, for restoring the disturbance rejection ability on resonant frequency, T_{VSG} is configured to move the Bode plot from the cyan curve to the blue curve. Next, for restoring the disturbance rejection ability on the full-band, K_{VSG} is configured to move the Bode plot from the blue curve to the red curve. Based on the two parameters 1000 and 50, the frequency deviations under the load disturbance are shown in Figure 7A, where the frequency nadir is restored and the RoCoF is retarded.

Considering the two control parameters T_{VSG} and K_{VSG} are both for regulat-

ing the operating power of IAC-VSGs, T_{VSG} and K_{VSG} can potentially be adjusted interchangeably. For analyzing this issue, Figure 7 also illustrates another scenario (i.e., $T_{\text{VSG}} = 200$ and $K_{\text{VSG}} = 90$). This scenario has a smaller T_{VSG} while a larger K_{VSG} compared with the previous scenario. It can be seen from Figure 7A that the frequency nadir Δf^{nadir} is the same in these two scenarios, while the RoCoF becomes steeper in the $(T_{\text{VSG}}, K_{\text{VSG}})$ scenario. The main reason is that the system equivalent inertia H in Equation (16) becomes smaller when decreasing T_{VSG} from 1000 to 200. These results verify that the two control parameters T_{VSG} and K_{VSG} can be adjusted interchangeably to restore the frequency nadir, while the RoCoF only depends on T_{VSG} . The significance for practical engineering application is that IAC-VSGs' control parameters can have wider adjustable ranges only when the power system retains large inertia. Otherwise, T_{VSG} should be configured first to guarantee adequate equivalent inertia H .

Impact Analysis on the Operation of IAC-VSGs. Figure 7C shows the IAC-VSG's regulation power in the two scenarios. The similarity is that the regulation power increases at first and then decreases to be even lower than zero. It means that IACs decrease the operating power at the beginning to support the power system's frequency, while they withdraw the regulation service and increase their operating power with the recovery of the power system's frequency. The reason is that the decreased operating power at the beginning causes the increase of indoor temperature, and IACs will consume power energy to restore the indoor temperature after withdrawing from the regulation service, as shown in Figure 7D.

However, there are also some differences in the two scenarios. In Figure 7C, the maximum regulation power is larger and the operating power returns to zero faster in the scenario $(T_{\text{VSG}}, K_{\text{VSG}})$, because T_{VSG} is essentially a

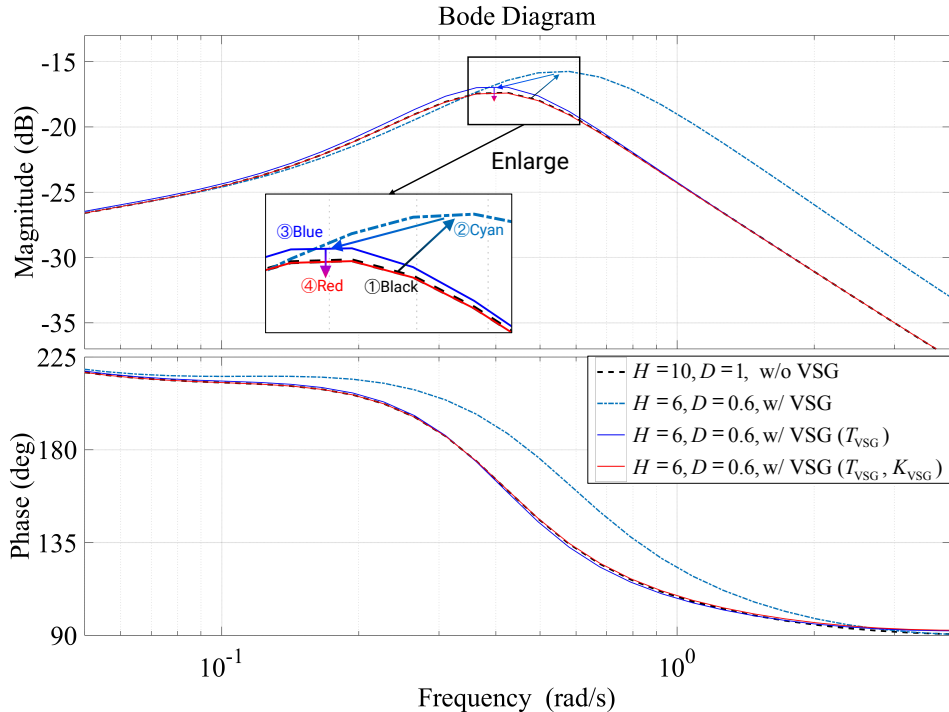


Figure 6. Bode plots of the power system with different inertia ratios.

APPENDIX B

The parameters of the IACs are based on the Chinese National Standards (GB/T 7725-2004, GB 12021.3-2010, GB 50411-2019) and some realistic test data, as follows: the available number of rooms and IACs is 110,000; the set temperature θ_i^{set} is distributed randomly among 22~26°C to represent various users' comfortable requirements; the ambient temperature is 35°C; the maximum indoor temperature deviation is 1°C; IACs' rated power P_i^N are distributed among 4.5~14kW according to the living area A_i ; the IAC's coefficient of performance is distributed among 3.0~3.6; the built-in controller $\varphi(s)$ adopts the proportional integral controller with the parameters of $0.12^{\circ}\text{C}^{-1}$ and $0.02^{\circ}\text{C}^{-1}\cdot\text{S}^{-1}$. Moreover, the thermal capacity C_i and resistance R_i of the room are obtained as:

$$\begin{cases} C_i = c_a \rho_a V_i = c_a \rho_a A_i h_i, \forall i \in I, \\ R_i = [U_h A_i^s]^{-1} = [U_h (2A_i + 4h_i \sqrt{A_i})]^{-1}, \forall i \in I \end{cases}$$

where $c_a = 1.005 \text{ kJ} \cdot \text{kg}^{-1} \cdot ^{\circ}\text{C}^{-1}$ and

derivative control for IAC-VSGs (i.e., the equivalent inertia is related to the RoCoF). The RoCoF is very large at the beginning of frequency deviations, which leads to a larger regulation power compared with the T_{vsg} scenario. By contrast, K_{vsg} is essentially a proportional control for IAC-VSGs, which plays a more important role after the fall time $\Delta t^{\text{recovery}}$. It causes the IAC's operating power recovers slowly in the K_{vsg} scenario. The regulation process continues until the system frequency deviations disappear. The regulation speed differences in the two scenarios also reflect in the indoor temperature dynamic process, as shown in Figure 7D. The indoor temperature recovers more slowly in the K_{vsg} scenario. However, no matter in which scenario, the users' comfortable indoor temperature constraints can always be guaranteed. The maximum deviations are only around 0.1°C and 0.2°C in the two scenarios, respectively.

CONCLUSIONS

The inertia and damping in RENs-dominated power systems are decreasing rapidly, leading to the deficiency of system's dynamic performance. To address this issue, this paper proposes the modelling and control methods of IAC-VSGs to enhance the system stability. By integrating IAC-VSGs into the power system model, we obtain the upgraded system equivalent inertia and damping, and thematically prove these two critical indexes can be enhanced by IAC-VSGs. Furthermore, this paper proposes an evaluation method of the system's dynamic performance based on the closed-loop transfer function in the complex frequency domain. On this basis, we design the parameter configuration method for IAC-VSGs' controllers to remedy the deficiency of the system's dynamic performance. The results verify that IAC-VSGs can be adjusted flexibly to alleviate the magnitude of system frequency deviations and the dropping speed of RoCoF remarkably. The users' comfortable indoor temperature constraints can also be guaranteed. This study utilizes naturally occurring load resources as VSGs to enhance the power system stability, which can provide valuable reference for maintaining the safe and stable operation of RENs-dominated power systems.

APPENDIX A

The parameters of the reheat steam synchronous generator are set as follows: the rated capacity S_j^g is 800MW; the generator inertia H_j^g is 10s; the time constants of the speed governor T_j^g , the turbine T_j^t , and the reheat process T_j^r are 0.2s, 7s and 0.3s, respectively; the high pressure turbine section F_j^{hp} is 0.3; the speed droop parameter R_j^g and the integral gain K_j^g are 0.05 and 0.5, respectively.

$\rho_a = 1.205 \text{ kg} \cdot (\text{m}^3)^{-1}$ are the heat capacity and density of the air, respectively; U_h is the heat transfer coefficient and equals to $3.6 \text{ W} \cdot (\text{m}^2 \cdot ^{\circ}\text{C})^{-1}$; V_i , A_i , h_i and A_i^s

are the volume, living area, height and surface area of the room, respectively. Each room's living area A_i is assumed to be a square and distributed among 60~140 m². All the rooms' height is assumed to be 2.5m. The volume and surface area of the room can be calculated as shown in Equation (26).

REFERENCES

- Zhou, Q., Li, Z., Wu, Q., & Shahidehpour, M. (2019). Two-stage load shedding for secondary control in hierarchical operation of islanded microgrids. *IEEE Trans. Smart Grid*, **10**(3):3103–3111. DOI:[10.1109/TSG.2018.2879741](https://doi.org/10.1109/TSG.2018.2879741)
- Shi, Q., Li, F., Kuruganti, T., Olama, M. M., Dong, J., Wang, X., & Winstead, C. (2021). Resilience-oriented DG siting and sizing considering stochastic scenario reduction. *IEEE Trans. Power Syst.*, **36**(4):3715–3727. DOI:[10.1109/TPWRS.2021.3070229](https://doi.org/10.1109/TPWRS.2021.3070229)
- Jiang, T., Sun, T., Liu, G., Li, X., Zhang, R., & Li, F. (2022). Resilience evaluation and enhancement for island city integrated energy systems. *IEEE Trans. Smart Grid*, Early Access. DOI:[10.1109/TSG.2022.3150804](https://doi.org/10.1109/TSG.2022.3150804).
- Zhou, Q., Shahidehpour, M., Li, Z., & Xu, X. (2019). Two-layer control scheme for maintaining the frequency and the optimal economic operation of hybrid AC/DC microgrids. *IEEE Trans. Power Syst.*, **34**(1):64–75. DOI:[10.1109/TPWRS.2018.2886871](https://doi.org/10.1109/TPWRS.2018.2886871)
- Mir, A. S., & Senroy, N. (2020). Self-tuning neural predictive control scheme for ultrabattery to emulate a virtual synchronous machine in autonomous power systems. *IEEE Trans. Neural Netw. Learn. Syst.*, **31**(1):136–147. DOI:[10.1109/TNNLS.2019.2900369](https://doi.org/10.1109/TNNLS.2019.2900369)
- Chen, T., Zhang, B., Pourbabak, H., Kavousi-Fard, A., & Su, W. (2018). Optimal routing and charging of an electric vehicle fleet for high-efficiency dynamic transit systems. *IEEE Trans. Smart Grid*, **9**(4):3563–3572. DOI:[10.1109/TSG.2017.2708499](https://doi.org/10.1109/TSG.2017.2708499)
- Zhang, X., Pipattanasompon, M., Chen, T., & Rahman, S. (2020). An IoT-based thermal model learning framework for smart buildings. *IEEE Internet Things J.*, **7**(1):518–527. DOI:[10.1109/IOT.2019.2921389](https://doi.org/10.1109/IOT.2019.2921389)
- Siano, P., & Sarno, D. (2016). Assessing the benefits of residential demand response in a real-time distribution energy market. *Appl. Energy*, **161**:533–551. DOI:[10.1016/j.apenergy.2015.08.019](https://doi.org/10.1016/j.apenergy.2015.08.019)
- Shao, C., Ding, Y., Siano, P., & Lin, Z. (2019). A framework for incorporating demand response of smart buildings into the integrated heat and electricity energy system. *IEEE Trans. Ind. Electron.*, **66**(2):1465–1475. DOI:[10.1109/TIE.2018.2834674](https://doi.org/10.1109/TIE.2018.2834674)
- Chen, G., Zhang, H., Hui, H., & Song, Y. (2021). Fast Wasserstein-distance-based distributionally robust chance-constrained power dispatch for multi-zone HVAC systems. *IEEE Trans. Smart Grid*, **12**(5):4016–4028. DOI:[10.1109/TSG.2021.3062303](https://doi.org/10.1109/TSG.2021.3062303)
- Lu, N. (2012). An evaluation of the HVAC load potential for providing load balancing service. *IEEE Trans. Smart Grid*, **3**(3):1263–1270. DOI:[10.1109/TSG.2012.2193230](https://doi.org/10.1109/TSG.2012.2193230)
- Chen, T., Cui, Q., Gao, C., Hu, Q., Lai, K., Yang, J., Lyu, R., Zhang, H., & Zhang, J. (2021). Optimal demand response strategy of commercial building-based virtual power plant

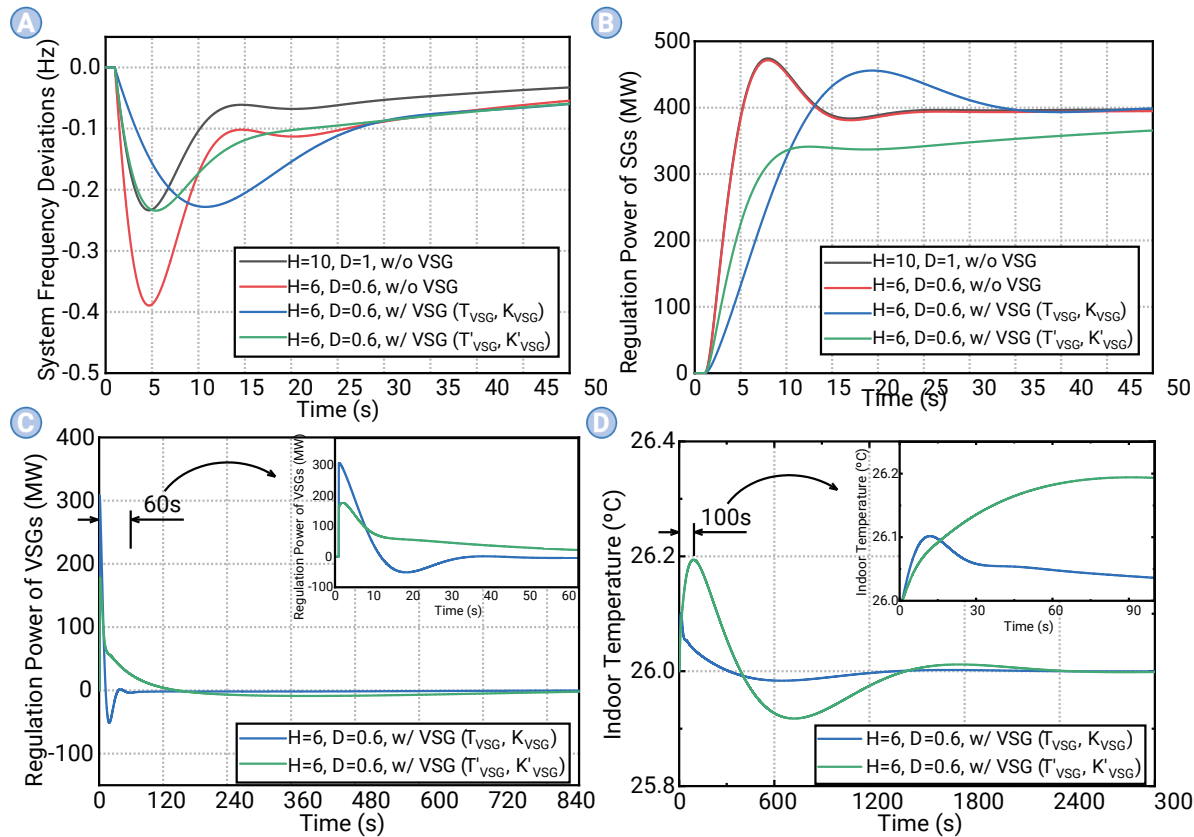


Figure 7. Regulation process of the power system under load disturbances. (A) System frequency deviations. (B) Regulation power of SGs. (C) Regulation power of IAC-VSG. (D) Indoor temperature deviations.

- using reinforcement learning. *IET Gener. Transm. Distrib.*, April 2021.
13. Song, M., Gao, C., Yan, H., & Yang, J. (2018). Thermal battery modeling of inverter air conditioning for demand response. *IEEE Trans. Smart Grid*, **9**(6):5522–5534. DOI:10.1109/TSG.2018.2797791
 14. Hong, J., Hui, H., Zhang, H., Dai, N., & Song, Y. (2022). Distributed control of large-scale inverter air conditioners for providing operating reserve based on consensus with nonlinear protocol. *IEEE Internet Things J.*, Early Access, February 2022.
 15. Hui, H., Ding, Y., & Zheng, M. (2018). Equivalent modeling of inverter air conditioners for providing frequency regulation service. *IEEE Trans. Ind. Electron.*, **66**(2):1413–1423. DOI:10.1109/TIE.2018.2822333
 16. Song, M., Sun, W., Shahidehpour, M., Yan, M., & Gao, C. (2021). Multi-time scale coordinated control and scheduling of inverter-based TCLs with variable wind generation. *IEEE Trans. Sustain. Energy*, **12**(1):46–57. DOI:10.1109/TSTE.2020.2996974
 17. Zhang, X., Biagioni, D., Cai, M., Graf, P., & Rahman, S. (2021). An edge-cloud integrated solution for buildings demand response using reinforcement learning. *IEEE Trans. Smart Grid*, **12**(1):420–431. DOI:10.1109/TSG.2021.3033140
 18. Kim, Y. (2018). Optimal price based demand response of HVAC systems in multizone office buildings considering thermal preferences of individual occupants. *IEEE Trans. Ind. Informat.*, **14**(11):5060–5073. DOI:10.1109/TII.2020.3033045
 19. Shi, Q., Chen, C., Mammoli, A., & Li, F. (2020). Estimating the profile of incentive-based demand response (IBDR) by integrating technical models and social-behavioral factors. *IEEE Trans. Smart Grid*, **11**(1):171–183. DOI:10.1109/TSG.2020.2971345
 20. Jiang, T., Wu, C., Zhang, R., Li, X., Chen, H., & Li, G. (2022). Flexibility clearing in joint energy and flexibility markets considering TSO-DSO coordination. *IEEE Trans. Smart Grid*, Early Access, February 2022.
 21. Hui, H., Ding, Y., Chen, T., Rahman, S., & Song, Y. (2021). Dynamic and stability analysis of the power system with the control loop of inverter air conditioners. *IEEE Trans. Ind. Electron.*, **68**(3):2725–2736. DOI:10.1109/TIE.2020.2972082
 22. Zhong, Q. (2016). Virtual synchronous machines: A unified interface for grid integration. *IEEE Power Electron. Mag.*, **3**(4):18–27. DOI:10.1109/MPEL.2016.2608285
 23. Othman, M. H., Mokhlis, H., Mubin, M., Talpur, S., Ab Aziz, N. F., Dradi, M., & Mohamad, H. (2020). Progress in control and coordination of energy storage system-based VSG: A review. *IET Renew. Power Gener.*, **14**(2):177–187. DOI:10.1049/rpg2.12067
 24. Bevrani, H., Ise, T., & Miura, Y. (2014). Virtual synchronous generators: A survey and new perspectives. *Int. J. Electr. Power Energy Syst.*, **54**:244–254. DOI:10.1016/j.ijepes.2013.07.016
 25. Zhang, J., & Xu, H. (2017). Online identification of power system equivalent inertia constant. *IEEE Trans. Ind. Electron.*, **64**(10):8098–8107. DOI:10.1109/TIE.2017.2754060
 26. Chen, M., Zhou, D., & Blaabjerg, F. (2020). Modelling, implementation, and assessment of virtual synchronous generator in power systems. *J. Mod. Power Syst. Clean Energy*, **8**(3):399–411. DOI:10.1007/s40565-019-00443-3
 27. Zhang, W., & Yan, X. (2020). Equivalence analysis of virtual synchronous machines and frequency-droops for inertia emulation in power systems with converter-interfaced renewables. *J. Electr. Eng. Technol.*, **15**(3):1167–1175. DOI:10.5370/JEET.2020.15.3.1167
 28. Wang, Y., Chen, Q., Hong, T., & Kang, C. (2019). Review of smart meter data analytics: Applications, methodologies, and challenges. *IEEE Trans. Smart Grid*, **10**(3):3125–3148. DOI:10.1109/TSG.2018.2856510
 29. Wang, J., Huang, S., Wu, D., & Lu, N. (2021). Operating a commercial building HVAC load as a virtual battery through airflow control. *IEEE Trans. Sustain. Energy*, **12**(1):158–168. DOI:10.1109/TSTE.2020.2997773
 30. Skogestad, S., Postlethwaite, I. (2007). Multivariable feedback control: Analysis and design. New York, NY, USA: Wiley.
 31. R, V., P, R., & M.P, S. (2018). A modified active power control scheme for enhanced operation of PMSG-based WGs. *IEEE Trans. Sustain. Energy*, **9**(2):630–638. DOI:10.1109/TSTE.2017.2784526
 32. Mir, A. S., & Senroy, N. (2019). Intelligently controlled flywheel storage for enhanced dynamic performance. *IEEE Trans. Sustain. Energy*, **10**(4):2163–2173. DOI:10.1109/TSTE.2019.2903039

FUNDING AND ACKNOWLEDGMENTS

This work was supported by National Natural Science Foundation of China and Science and Technology Development Fund, Macao SAR.

AUTHOR CONTRIBUTIONS

All authors contributed to the manuscript and approved the final version.

DECLARATION OF INTERESTS

The authors declare no competing interests.

DATA AND CODE AVAILABILITY

Data are available from the corresponding author upon reasonable request.

SUPPLEMENTAL INFORMATION

Supplementary materials are available at: <https://doi.org/10.59717/ijp.energy-use.2025.100009>